

# Enhancing inflationary model predictions via refined slow-roll dynamics

Debottam Nandi<sup>1,2,\*</sup>, Simran Yadav<sup>2,†</sup> and Manjeet Kaur<sup>2,‡</sup>

<sup>1</sup>*Center for Cosmology and Science Popularization (CCSP),*

*SGT University, Gurugram, Delhi-NCR, Haryana-122505, India*

<sup>2</sup>*Department of Physics and Astrophysics, University of Delhi, Delhi 110007, India*

The inflationary paradigm not only addresses early universe puzzles but also aligns well with the observational constraints, with slow-roll inflationary models fitting the best. Evaluating these model predictions requires considering both slow-roll inflationary dynamics and the subsequent reheating epoch. This involves the quantitative analysis that takes into account the effective equation of state (EoS) and duration of reheating, connecting these with the perturbations generated deep during the inflationary era. Given the complexities involved, many approximations are often used for simplification. However, as future observations are expected to improve the accuracy of these observables significantly, this work takes a different approach. Instead of relying on approximations, and instead of looking into the complex effects of (pre-)reheating, we focus on the corrections arising purely from more accurate analytical evaluations of the perturbations generated during the inflationary era itself. This is because the reheating dynamics is model-dependent and lack a single concrete analytical description, and thus introduce large uncertainties, making robust predictions difficult. In this article, we mainly incorporate two improvements: the first is the accurate dynamics of the slow-roll evolution, and, thus, the end of inflation; and the second is the higher-order slow-roll corrections to the perturbed observables. Our findings indicate that, by implementing these corrections, the theoretical predictions improve significantly. It also indicates that seemingly minor corrections can have significant effects on the perturbed observables and these refined predictions can be compared with future observations to potentially rule out models and help resolve the degeneracy problem of the inflationary paradigm.

Keywords: The Early Universe, Inflationary Paradigm, Reheating, CMBR, Perturbations.

## I. INTRODUCTION

The inflationary paradigm [1–31], which describes a brief period of accelerated expansion, is the most successful framework for explaining the dynamics of the early universe. Within this

---

\* [debottam\\_ccsp@sgtuniversity.org](mailto:debottam_ccsp@sgtuniversity.org)

† [simranyadavkhola@gmail.com](mailto:simranyadavkhola@gmail.com)

‡ [mkaur1@physics.du.ac.in](mailto:mkaur1@physics.du.ac.in)

paradigm, slow-roll inflation involves field(s) slowly rolling down the potential, resulting in near-exponential expansion and providing an explanation for the observational constraints [32–35]. As the field(s) approaches the bottom of the potential, inflation ends, and shortly afterward, the field(s) begins to oscillate around this minimum. This phase, known as the reheating epoch, involves the inflaton field(s) coupling with and decaying into other standard particles, leading to the onset of the radiation-dominated era [36–58].

Theoretical constraints derived from an inflationary model, however, not only depend on the dynamics of inflation itself but also depend on the reheating era, and therefore, studying reheating dynamics is crucial for accurately predicting the early universe behavior. There are two main approaches to this: the first is the qualitative analysis [36–43, 46] which examines the exact decay process of the inflaton field through the parametric resonance, leading to the understanding of the microphysics involved during the reheating epoch. The second approach, which is the main focus of this manuscript, is the quantitative analysis [44, 45, 47, 49, 52, 54, 59–64]. This approach looks at the macrophysics of the reheating epoch by constraining the duration ( $N_{\text{re}}$ ) and the equation of state (EoS) parameter ( $w_{\text{re}}$ ) during the reheating era using perturbations generated deep in the early (inflation) universe.

In this analysis, the Hubble horizon and the associated length scales are used to constrain the duration when the pivot scale exits the Hubble horizon from the end of inflation, i.e.,  $N_k$ , and the reheating parameters ( $N_{\text{re}}$ ,  $w_{\text{re}}$ ). Given any model, using  $N_k$ , one can determine both the scalar and tensor perturbations associated with the pivot scale and compare this with the observations. Thus, the theoretically obtained perturbed observables, namely the scalar-spectral index  $n_s$  and the tensor-to-scalar ratio  $r$  are heavily dependent on the reheating parameters  $N_{\text{re}}$  and  $w_{\text{re}}$ . Since the perturbations ( $n_s$  and  $r$ ) are highly sensitive to  $N_k$ , and consequently, to ( $N_{\text{re}}$ ,  $w_{\text{re}}$ ), even small corrections or deviations in  $N_k$  or reheating parameters can significantly improve  $n_s$ . Ongoing experiments [32–35] already measure  $n_s$  with an accuracy of  $\Delta n_s \sim 10^{-2}$  and upcoming experiments like PRISM [65], EUCLID [66], cosmic 21-cm surveys [67], and CORE experiments [68] are projected to improve this accuracy to  $\Delta n_s \sim 10^{-3}$ . Therefore, taking advantage of this, in this work, we focus on refining the analysis itself to obtain tighter constraints on the inflationary paradigm, as the analysis relies on numerous approximations. This refined approach, in turn, can help resolve the degeneracy problem of the inflationary paradigm [25, 69–71] by eliminating more inflation models.

Improving the analysis can again be performed in two main ways. The first one involves a detailed and careful consideration of the reheating analysis that can accurately depict the reheat-

ing parameters  $(N_{\text{re}}, w_{\text{re}})$ . However, since it entails dealing with various distinct microphysical processes — requiring largely model-dependent treatment known as the qualitative analysis — and consequently introduces substantial uncertainties. For this reason, we have opted not to pursue this approach as it is beyond the scope of this work. Instead, we focus on the second, more straightforward improvement: the slow-roll methodology and approximations with a brief and simplest quantitative reheating epoch with constant  $w_{\text{re}}$ . Recent findings in Refs. [72, 73] indicate that a near-accurate analytical solution can significantly enhance background predictions near the end of inflation, thereby improving  $N_k$  [72]. For example, in the case of Starobinsky inflation, the improvement  $\Delta N_k \sim 1.5$  suggests that

$$n_s \sim 1 - \frac{2}{N_k}, \quad \Delta n_s \sim \frac{\Delta N_k}{N_k^2} \sim 10^{-3}.$$

In addition to leading-order slow-roll approximations, higher-order slow-roll corrections [74–88] can be considered to further improve the evaluation of perturbed observables such as  $n_s$  and  $r$ . Therefore, the objective of this work is to enhance the model predictions by implementing both the improved near-accurate dynamics and higher-order slow-roll corrections and comparing our results with the existing literature. As an example, we consider the most popular inflationary model: the Starobinsky model of inflation [1, 2, 8, 89, 90]. Using the conventional leading order analytical approximation, the constraint on  $n_s$  is:  $0.9613 \leq n_s \leq 0.9641$ , which leads to further constrain  $N_{\text{re}} \leq 16$  (equivalently, the energy at the end of reheating, i.e.,  $T_{\text{re}} \geq 10^{10}$  GeV, assuming  $w_{\text{re}} = 0$ ). However, after implementing the accurate dynamics as well as the higher-order slow-roll corrections, the bounds on these parameters change significantly, and the new constraint on  $n_s$  for numerical solution becomes:  $0.9613 \leq n_s \leq 0.9649$ , which leads to further constrain  $N_{\text{re}} \leq 21$  (and subsequently,  $T_{\text{re}} \geq 10^8$  GeV), while for higher-order corrections these become:  $0.9613 \leq n_s \leq 0.9653$ , constraints on reheating parameters are,  $N_{\text{re}} \leq 24$  and  $T_{\text{re}} \geq 10^7$ , which has the potential to rule out the model from future observations. The result is unexpected, as one might anticipate the corrections to be negligible. Thus, instead of relying on the conventional approximation method, our results demonstrate the critical need for corrections due to the accurate dynamics in each model of inflation, which may lead to a significant change in theoretical predictions and potentially rule out models from observations. This implies that even seemingly minor improvements to the background dynamics can have a substantial impact on the theoretically obtained perturbed observables, which must not be ruled out without verification.

The article is structured as follows: the following section II presents the model and the subsequent dynamics for the early universe dynamics. In this section, we also demonstrate the slow-roll

conditions as well as the slow-roll approximations. In the subsequent section III, we study the quantitative analysis of reheating linking the inflationary perturbed variables to the observable constraints. This section, as an example, also examines the popular Starobinsky model of inflation, and with the help of the reheating analysis along with leading-order slow-roll approximations, we carefully obtain the observational consequences of the model. In Sec. IV, we highlight the dire need for the corrections to the dynamics, subsequently implement these changes, and obtain the improved constraint of the model, which turns out to be significant. Finally, we conclude our work in Sec. V.

A brief explanation about some terms and symbols we'll be using. In our work, we use natural units where  $\hbar = c = k_B = 1$ . We also define the reduced Planck mass as  $M_{\text{pl}} \equiv (8\pi G)^{-1/2} = 1$ . The metric signature we use is  $(-, +, +, +)$ . Greek indices are contracted with the metric tensor  $g_{\mu\nu}$ , while Latin indices will be contracted with the Kronecker delta  $\delta_{ij}$ . We use symbols  $\partial$  and  $\nabla$  for partial and covariant derivatives, respectively. Additionally, the dots and primes above symbols represent derivatives for cosmic and conformal time, respectively, related to the Friedmann-Lemaître-Robertson-Walker (FLRW) line-element.

## II. GENERAL EQUATIONS AND SLOW-ROLL CONDITIONS

In this section, we discuss the general equations and solutions for a slow-roll inflationary universe. For that, let us consider the simplest action with a single canonical scalar field  $\phi$  minimally coupled to gravity with a potential  $V(\phi)$ , which can be written as

$$S = \frac{1}{2} \int d^4x \sqrt{-g} (R - g^{\mu\nu} \partial_\mu \phi \partial_\nu \phi - 2V(\phi)). \quad (1)$$

Here,  $R$  is the Ricci scalar. The corresponding equations of motion, i.e., Einstein's equations and the equation of the scalar field, can be written as

$$R_{\mu\nu} - \frac{1}{2} g_{\mu\nu} R = T_{\mu\nu(\phi)}, \quad (2)$$

$$\nabla_\mu T^{\mu\nu}_{(\phi)} = 0, \quad (3)$$

where  $T^{\mu}_{\nu(\phi)}$  is the stress-energy tensor corresponding to the  $\phi$  field and can be written as

$$T_{\mu\nu(\phi)} = \partial_\mu \phi \partial_\nu \phi - g_{\mu\nu} \left( \frac{1}{2} \partial_\lambda \phi \partial^\lambda \phi + V(\phi) \right). \quad (4)$$

Using the flat FLRW line element describing the homogeneous and isotropic universe at large scales, i.e.,

$$ds^2 = -dt^2 + a^2(t) d\mathbf{x}^2, \quad (5)$$

where,  $a(t)$  is the scalar factor, Eqs. (2) and (3) can be reduced to

$$3H^2 = \frac{1}{2}\dot{\phi}^2 + V(\phi), \quad (6)$$

$$\dot{H} = -\frac{1}{2}\dot{\phi}^2, \quad (7)$$

$$\ddot{\phi} + 3H\dot{\phi} + V_{,\phi} = 0. \quad (8)$$

where,  $H \equiv \dot{a}/a$  is the Hubble parameter, and  $A_x \equiv \partial A/\partial x$ . These equations can be re-defined in terms of the e-fold variable  $N \equiv \int H dt = \ln(a/a_0)$  as

$$H = \sqrt{\frac{V}{3 - \frac{1}{2}\phi_N^2}}, \quad \frac{H_N}{H} = -\frac{1}{2}\phi_N^2, \quad (9)$$

$$\phi_{NN} + \left(3 - \frac{1}{2}\phi_N^2\right) \left(\phi_N + \frac{V_{,\phi}}{V}\right) = 0, \quad (10)$$

where,  $A_{xx} = \partial^2 A/\partial x^2$ . Given a potential  $V(\phi)$ , one can solve the above equations to correctly obtain the dynamics of the early universe. Once the background equations are solved, one can in principle, solve the scalar ( $\mathcal{R}_k$ ) and tensor ( $h_k$ ) perturbations and evaluate the power spectra:

$$\mathcal{P}_{\mathcal{R}} = \frac{k^3}{2\pi^2} |\mathcal{R}_k|^2 \equiv A_{\mathcal{R}} \left(\frac{k}{k_*}\right)^{n_s-1}, \quad \mathcal{P}_T = 2 \cdot \frac{k^3}{2\pi^2} |h_k|^2 \equiv A_T \left(\frac{k}{k_*}\right)^{n_T} \quad (11)$$

where,  $k_*$  is the pivot scale,  $A_{\mathcal{R}}$ ,  $A_T$  are the scalar and tensor spectral amplitude,

$$n_s \equiv \left. \frac{d \ln \mathcal{P}_{\mathcal{R}}}{d \ln k} \right|_{k=k_*}, \quad n_T \equiv \left. \frac{d \ln \mathcal{P}_T}{d \ln k} \right|_{k=k_*}$$

are the scalar and tensor spectral index and and

$$r \equiv \frac{A_T}{A_{\mathcal{R}}}$$

is defined as the tensor-to-scalar ratio, which we compare with the observations. The current observations (PLANCK [32, 33, 35], BICEP/Keck [34]) suggest that, at the pivot scale ( $k_* = 0.05 \text{ Mpc}^{-1}$ ), the amplitude of the scalar power spectrum is  $A_{\mathcal{R}} \simeq 2.101_{-0.034}^{+0.031} \times 10^{-9}$  (68% CL) with the scalar spectral index being  $n_s = 0.9672 \pm 0.0059$  (68% CL), while the ratio ( $r$ ) of the tensor-to-scalar perturbation amplitudes is bounded by  $r < 0.028$  (95% CL). These observations agree remarkably well with the predictions of a near-scale-invariant spectrum of density perturbations in the inflationary paradigm. In the next section, we will discuss in detail, how, without explicitly evaluating the perturbations, one can obtain these observables using the background solutions in the case of slow-roll inflation.

### Slow-roll inflation

Let us first define the two slow-roll parameters  $\epsilon_1$  and  $\epsilon_2$  as

$$\epsilon_1 \equiv -\frac{\dot{H}}{H^2} = \frac{1}{2}\dot{\phi}_N^2, \quad \epsilon_2 \equiv \frac{\dot{\epsilon}_1}{H\epsilon_1} = 2\frac{\phi_{NN}}{\phi_N}. \quad (12)$$

The first variable  $\epsilon_1 < 1$  ensures that the universe is accelerating. On the other hand, the second variable  $\epsilon_2 \ll 1$  ensures the sufficient duration of the inflationary phase. In the case of slow-roll, both these parameters are extremely small, i.e.,

$$\epsilon_1 \ll 1, \quad \epsilon_2 \ll 1. \quad (13)$$

These two conditions are also referred to as slow-roll conditions. Under these conditions, Eqs. (9) and (10) become

$$H^2 \simeq \frac{1}{3}V, \quad \phi_N \simeq -\frac{V_\phi}{V}, \quad (14)$$

and the slow-roll parameters can be re-expressed in terms of the shape of the potential as

$$\epsilon_1 \simeq \frac{1}{2} \left( \frac{V_\phi}{V} \right)^2, \quad \epsilon_2 \simeq 2 \left( \frac{V_\phi^2}{V^2} - \frac{V_{\phi\phi}}{V} \right). \quad (15)$$

Eqs. (14) are referred to as the slow-roll equations. By solving these simplified equations, one can obtain the approximate analytical solution of the Hubble parameter as well as the slow-roll parameters, and thus the dynamics of the universe in the slow-roll regime.

In order to check for consistency with the observation, one can, in principle, obtain the observables corresponding to the perturbations associated with the pivot scale  $k$  in terms of slow-roll parameters as

$$A_{\mathcal{R}} \simeq \frac{H^2}{8\pi^2\epsilon_1}, \quad n_s \simeq 1 - 2\epsilon_1 - \epsilon_2, \quad r \simeq 16\epsilon_1. \quad (16)$$

The above expressions are obtained using the leading-order slow-roll approximation, assuming that higher-order contributions are heavily suppressed. Please note that these observables depend on the time variable  $N_k$ , representing the duration between the end of inflation and the epoch when the pivot scale  $k$  leaves the Hubble horizon. Typically, this duration is considered to be  $N_k \sim 50 - 60$ . However, it is a model-dependent quantity and in order to obtain the exact duration  $N_k$ , one must consider the post-inflationary dynamics, i.e., the reheating epoch. In the very next section, we will focus on this, which is also known as the quantitative analysis of reheating.

### III. QUANTITATIVE ANALYSIS OF REHEATING

As mentioned in the previous section, in the slow-roll regime, the slow-roll parameters are very small, i.e.,  $\epsilon_1, \epsilon_2 \ll 1$ . However, as the field rolls down the potential, these slow-roll parameters increase, and the inflation ends as soon as this condition is violated, i.e.,  $\epsilon_1 = 1$ . Briefly, after the end of inflation, the field reaches the bottom and begins to oscillate around it and couples with the other (standard) particles. As a consequence, at this stage, the time average of kinetic energy is the same as the average of the potential energy, and the field decays. This epoch is known as the reheating phase.

This epoch involves intricate microphysical processes and is largely model-dependent. As a result, any analytical extension of its dynamics carries substantial uncertainties, making it extremely challenging to describe the epoch through a single, unified analytical framework. To circumvent this difficulty and achieve a model-independent treatment, a simplified quantitative approach has been developed in which the equation-of-state parameter during the entire reheating epoch, i.e.,  $w_{\text{re}}$  is assumed to remain constant. Although this approximation does not capture the full microphysical complexity of reheating, it provides a useful macrophysical description that successfully connects inflationary predictions with observations and thereby enables broad, indirect constraints on the reheating scenario. In this case, the energy density during reheating effectively behaves as

$$\rho \propto a^{-3(1+w_{\text{re}})}. \quad (17)$$

We also define the duration of reheating  $N_{\text{re}}$  as

$$N_{\text{re}} \equiv \ln \left( \frac{a_{\text{re}}}{a_{\text{end}}} \right) \quad (18)$$

where  $a_{\text{end}}, a_{\text{re}}$  are the scale factor solutions at the end of the inflation and reheating epoch, respectively. In order to calculate the duration  $N_{\text{re}}$ , let us compare the mode of interest with the present scale as

$$\frac{k}{a_0 H_0} = \frac{a_k H_k}{a_0 H_0} = \frac{a_k}{a_{\text{end}}} \frac{a_{\text{end}}}{a_{\text{re}}} \frac{a_{\text{re}}}{a_{\text{eq}}} \frac{a_{\text{eq}}}{a_0} \frac{H_k}{H_{\text{eq}}} \frac{H_{\text{eq}}}{H_0}, \quad (19)$$

where  $k$  is the comoving scale, and (eq) and (0) denote the quantities at the matter-radiation equality and the present epoch, respectively. Then the above equation leads to:

$$\ln \left( \frac{k}{a_0 H_0} \right) = -N_k - N_{\text{re}} - N_{\text{RD}} + \ln \left( \frac{a_{\text{eq}} H_{\text{eq}}}{a_0 H_0} \right) + \ln \left( \frac{H_k}{H_{\text{eq}}} \right), \quad (20)$$

where  $N_k \equiv \ln \left( \frac{a_k}{a_{\text{end}}} \right)$ ,  $N_{\text{RD}} \equiv \ln \left( \frac{a_{\text{re}}}{a_{\text{eq}}} \right)$ . At the end of reheating, the energy density is

$$\rho_{\text{re}} = \frac{\pi^2}{30} g_{\text{re}} T_{\text{re}}^4 \quad (21)$$

where,  $g_{\text{re}}$  is the effective number of relativistic species upon thermalization. Radiation drives the ensuing expansion, with non-relativistic matter and dark energy making recent additions. Assuming a negligible entropy shift following  $T_{\text{re}}$ , the current CMB and neutrino background both retain the reheating entropy, which leads to the relation,

$$g_{\text{s, re}} T_{\text{re}}^3 = \left( \frac{a_0}{a_{\text{re}}} \right)^3 \left( 2T_0^3 + 6 \times \frac{7}{8} T_{\nu 0}^3 \right), \quad (22)$$

where the present (CMB) temperature,  $T_0 \simeq 2.73$  K, the neutrino temperature,  $T_{\nu 0} = (4/11)^{1/3} T_0$ , and  $g_{\text{s, re}}$  is the effective number of species for entropy at reheating. Therefore,  $T_{\text{re}}$  can be written as the present temperature  $T_0$  as

$$\frac{T_{\text{re}}}{T_0} = \frac{a_0}{a_{\text{eq}}} \frac{a_{\text{eq}}}{a_{\text{re}}} \left( \frac{43}{11g_{\text{s, re}}} \right)^{1/3}, \quad (23)$$

and the Eq. (20) can be re-written as

$$N_{\text{re}} = \frac{4}{1 - 3w_{\text{re}}} \left( -N_k - \frac{1}{4} \ln \left( \frac{30}{\pi^2 g_{\text{re}}} \right) - \frac{1}{3} \ln \left( \frac{11g_{\text{s, re}}}{43} \right) - \ln \left( \frac{k}{a_0 T_0} \right) - \frac{1}{4} \ln \rho_{\text{end}} + \ln H_k \right). \quad (24)$$

and  $T_{\text{re}}$  can be reduced to the following form:

$$T_{\text{re}} = \frac{a_0 T_0}{k} \left( \frac{43}{11g_{\text{s, re}}} \right)^{1/3} H_k e^{-N_k - N_{\text{re}}}. \quad (25)$$

where  $H_k$  can be written as

$$H_k = \frac{\pi \sqrt{r A_{\mathcal{R}}}}{\sqrt{2}}. \quad (26)$$

Please note that the Hubble parameter  $H_k$  is a function of duration  $N_k$ , and therefore,  $N_{\text{re}}$  is eventually a function of  $N_k$ . As spectral index  $n_s$  (or any time-dependent parameters like the field  $\phi$  or tensor-to-scalar ratio  $r$ ) depends on  $N_k$ , considering  $\{g_{\text{re}}, g_{\text{s, re}}\} \sim 100$ , one can plot  $n_s$  vs.  $N_{\text{re}}$  (or  $T_{\text{re}}$  from the above expression) and obtain strict constraint on  $N_{\text{re}}$  [25, 47, 53, 55, 59, 91, 92] as  $n_s$  is strictly bounded. This is referred to as the quantitative analysis of reheating. In the next section, we will elaborately discuss this analysis by implementing it on the Starobinsky model of inflation.



### A. Starobinsky inflation

One of the most successful models of slow-roll inflation is the Starobinsky model [1, 2, 8, 89, 90] where the potential in the Einstein frame is given by:

$$V(\phi) = \frac{3}{4}M^2 \left(1 - e^{-\sqrt{2/3}\phi}\right)^2, \quad (27)$$

where  $M$  is the mass of the scalar field  $\phi$ . Assuming the slow-roll conditions are satisfied, we can

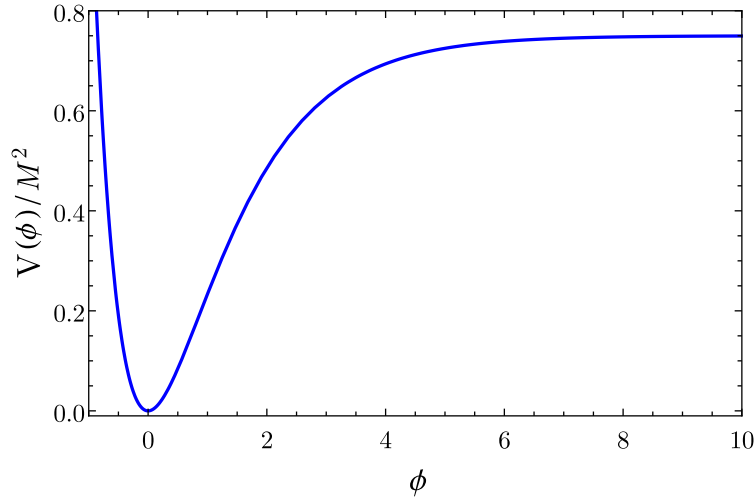


FIG. 1. The Starobinsky potential given in Eq. (27).

immediately obtain the two slow-roll equations (i.e., Eqs. (14)) as

$$H \simeq \frac{M}{2} \left(1 - e^{-\sqrt{2/3}\phi}\right), \quad \phi_N \simeq -2\sqrt{\frac{2}{3}} \frac{e^{-\sqrt{2/3}\phi}}{\left(1 - e^{-\sqrt{2/3}\phi}\right)}, \quad (28)$$

and the slow-roll parameters can be expressed in terms of the field  $\phi$  as (i.e., Eqs. (15)):

$$\epsilon_1 \simeq \frac{4e^{-2\sqrt{2/3}\phi}}{3\left(1 - e^{-\sqrt{2/3}\phi}\right)^2}, \quad \epsilon_2 \simeq \frac{8e^{-\sqrt{2/3}\phi}}{3\left(1 - e^{-\sqrt{2/3}\phi}\right)^2}. \quad (29)$$

With the help of Eq. (28), one can easily solve the scalar field solution in terms of the e-folding number  $N_k$ , and the solutions of the slow-roll parameters at the leading order can be obtained as:

$$\epsilon_1 \simeq \frac{3}{4N_k^2}, \quad \epsilon_2 \simeq \frac{2}{N_k}, \quad (30)$$

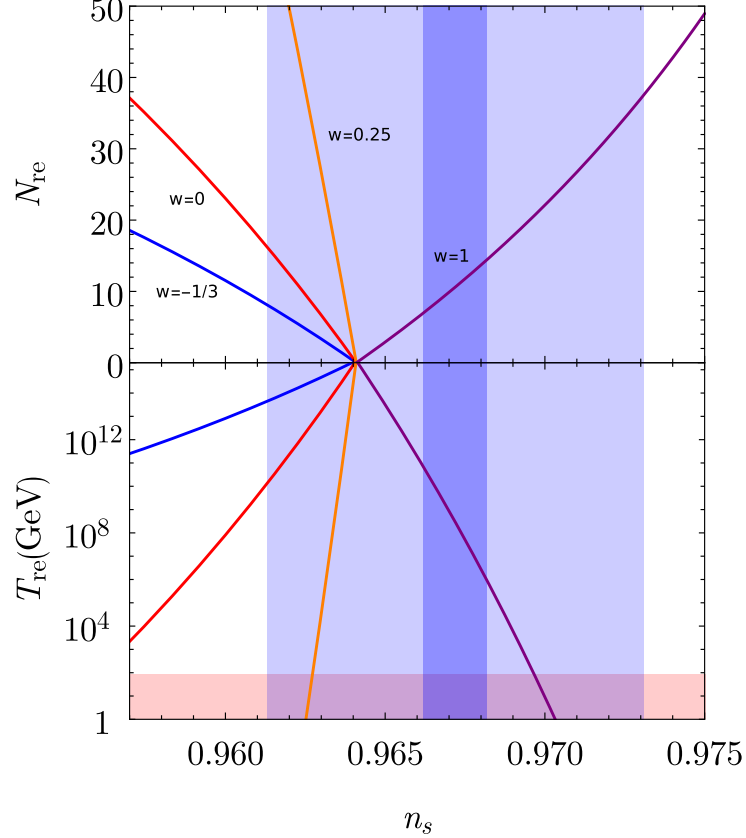


FIG. 2. We plot the duration of reheating  $N_{\text{re}}$  and reheating temperature  $T_{\text{re}}$  given in Eqs. (24) and (25) as functions of the scalar spectral index  $n_s$  given by Eq. (31) using leading order slow-roll approximations for the case of Starobinsky inflation. Please note that different colors represent dynamics corresponding to different effective EoS parameter  $w_{\text{re}}$  as indicated in the figure. The blue-shaded region represents the  $1\sigma$  constraint on the value of  $n_s$  using ongoing observations [32–35] with  $n_s = 0.9672 \pm 0.0059$ . The dark blue region shows the future projected bound on  $n_s$  with a sensitivity of  $10^{-3}$ , assuming its central value remains unchanged. The temperature below the lighter red region is excluded due to the constraint from the electroweak scale, which is taken to be 100 GeV.

and, using the leading order slow-roll approximation, i.e., Eqs. (16), we can quickly evaluate the scalar spectral index and the tensor-to-scalar ratio in terms of the e-folding number as:

$$n_s \simeq 1 - \frac{2}{N_k}, \quad r \simeq \frac{12}{N_k^2}. \quad (31)$$

Using the above equation along with Eqs. (24) and (25), one can obtain parametric dependence of  $N_{\text{re}}$  and  $T_{\text{re}}$  on  $n_s$ . In the case of the Starobinsky model, this is shown in Fig. 2. Keep in mind that,  $N_{\text{re}} \geq 0$ , with  $N_{\text{re}} \ll 1$  is referred to as instantaneous reheating [92, 93]. It immediately leads to the constraint on the value of  $n_s$ . For example, considering that during reheating, the evolution of the universe effectively behaves as matter-expansion, i.e.,  $w_{\text{re}} = 0$ . Thus, in the  $1\sigma$  domain, we

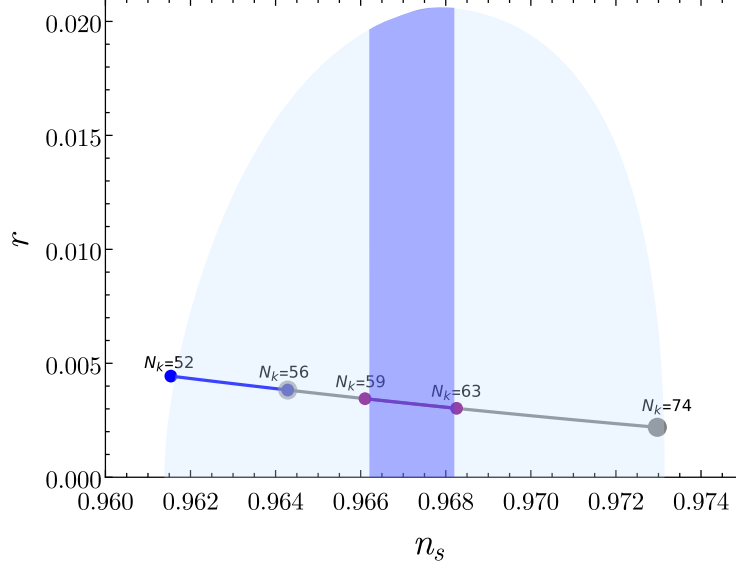


FIG. 3. We plot the inflationary observables, tensor-to-scalar ratio ( $r$ ) as a function of scalar spectral index ( $n_s$ ) for the Starobinsky model using leading order slow-roll approximations given by Eq. (31). This evolution is presented considering the bound on duration  $N_k$  using the reheating regime. We consider different EoS parameters during reheating  $w_{\text{re}}$  and observe the constraint on the duration  $N_k$ . Correspondingly, in the figure, blue line corresponds to the bound for  $w_{\text{re}} < 1/3$ , the gray line for  $w_{\text{re}} > 1/3$  and the purple line for the future observational bound of  $n_s$ . The blue-shaded region represents the  $1\sigma$  constraint on the value of  $n_s$  using ongoing observations [32–35] with  $n_s = 0.9672 \pm 0.0059$ . The dark blue region shows the future projected bound on  $n_s$  with a sensitivity of  $10^{-3}$ , assuming its central value remains unchanged.

get the bound on  $N_k$  as

$$52 \leq N_k \leq 56 \quad (32)$$

and correspondingly, the bound on  $n_s$  becomes:

$$0.961 \leq n_s \leq 0.964 \quad (33)$$

In fact, as can be seen, for  $w_{\text{re}} < 1/3$ , it is obvious that there is an upper bound on  $N_k$ , which implies a bound on  $n_s$  as well, i.e.,  $N_k \leq 56$  and  $n_s < 0.964$ . It also immediately puts a tight constraint on  $N_{\text{re}}$  and  $T_{\text{re}}$  (for  $w_{\text{re}} = 0$ ) as

$$N_{\text{re}} \leq 16, \quad T_{\text{re}} \geq 10^{10} \text{ GeV}. \quad (34)$$

However, during reheating, if we assume  $w_{\text{re}} > 1/3$ , these constraints flip and in the  $1\sigma$  domain, there arises a new bound with a lower value of  $N_k$  as well as in  $n_s$  as

$$56 \leq N_k \leq 74, \quad 0.964 \leq n_s \leq 0.973. \quad (35)$$

Consequently, the bound on reheating parameters becomes (for  $w_{\text{re}} = 1$ )

$$N_{\text{re}} \leq 37, \quad T_{\text{re}} \geq 10^{-9} \text{ GeV}. \quad (36)$$

Considering these bounds into account, we plot  $r$  as a function of  $n_s$  in Fig. 3. Further, instead of looking in  $1\sigma$  limit, if we consider the observational constraints proposed by the forthcoming experiments such as PRISM [94] and EUCLID [95], cosmic 21-cm surveys [67], and CORE experiments [68], which offer a precision enhancement of  $10^{-3}$  in  $n_s$ , the constraints on  $N_k$ ,  $N_{\text{re}}$  and  $T_{\text{re}}$  can be substantially improved<sup>1</sup>. Then one can immediately refer from the Fig. 2 and 3 that for  $w_{\text{re}} < 1/3$ , the scalar spectral index does not satisfy the constraints in  $1\sigma$  level posed by future observations. Therefore, under these conditions, this model can be ruled out. The model can be survived if one assumes  $w_{\text{re}} > 1/3$ , and the bound on  $N_{\text{re}}$  and  $T_{\text{re}}$  for the constraints posed by future observations becomes

$$7 \leq N_{\text{re}} \leq 14, \quad 10^9 \text{ GeV} \geq T_{\text{re}} \geq 10^6 \text{ GeV}. \quad (37)$$

Even in that case, if the future observations detect instantaneous reheating [92, 93], i.e.,  $N_{\text{re}} \ll 1$ ,  $n_s$  appears to be outside of the contour from the future observations. Therefore, unless  $w > 1/3$  with the prolonged reheating era, the analytical approximation may lead to ruling out the Starobinsky inflation model. However, keeping aside the future observations, in the next section, we will see a significant improvement in these constraints by implementing meaningful corrections to the dynamics rather than the analytical approximations.

#### IV. NUMERICAL IMPROVEMENTS

In the previous section, we discussed the CMB constraints on various inflationary models, which depend on the effective EoS parameter  $w_{\text{re}}$  as well as the duration of the reheating epoch  $N_{\text{re}}$ . There are two issues associated with this analysis. First, around and at the end of inflation, the slow-roll approximation breaks down. Yet, in evaluating duration  $N_k$  as well as energy density at end of inflation  $\rho_{\text{end}}$  in Eq. (24), we rely upon slow-roll approximations. Second, in evaluating perturbed observables in Eqs. (16), we consider only the leading-order contributions and ignore higher-order contributions, assuming their impact to be negligible. However, as anticipated in Refs. [72, 73], considering accurate dynamics rather than the slow-roll approximations may lead to notable enhancements in these predictions. Additionally, one can consider the onset of reheating

---

<sup>1</sup> The central value of  $n_s$  is assumed to be 0.9672 [35]

not at the end of inflation but at the bottom of the potential, as will be discussed in the subsequent section. The implementation and, therefore, the resulting corrections due to these considerations can be categorized into three parts:

1. Implementation of accurate inflationary dynamics through numerical methods instead of slow-roll approximations.
2. Implementation of higher-order slow-roll approximations instead of leading-order slow-roll approximations.
3. Implementation of onset of reheating as the bottom of the potential instead of the end of inflation.

In the following sections, we will conduct a detailed study of the impact of each of these corrections on the observational constraints. We will also compare the cumulative effects of these corrections with the existing predictions presented in the previous section.

#### A. Implementation of accurate inflationary dynamics through numerical methods

As mentioned earlier, this epoch of the slow-roll regime lasts as long as both of the slow-roll parameters are small, i.e., ( $\epsilon_1 \ll 1$ ,  $\epsilon_2 \ll 1$ ). On the other hand,  $\epsilon_1 = 1$  signals the end of inflation. It turns out that even before the end of inflation, these slow approximations break down. Despite this, we still rely on (leading-order) slow-roll approximations even at the end of inflation to determine the analytical solution of the background variables, assuming the contribution due to accurate dynamics in evaluating perturbed observables is negligible. However, it is crucial, as in this section, we shall learn the significance of obtaining the accurate values of not only the background parameters but also the end of inflation. To illustrate this, let's now discuss this in detail with an example: the Starobinsky inflation.

Using leading-order slow-roll approximations and solving the slow-roll equations (*viz.* Eqs. (14)):

$$H^2 \simeq \frac{V}{3}, \quad \phi_N \simeq -\frac{V_\phi}{V},$$

with the initial condition  $\phi_i = 5.8$ , we obtain the following results:

$$N_{\text{end}} \simeq 80.86, \quad \phi_{\text{end}} \simeq 0.94, \quad H_{\text{end}} \simeq 0.267 M, \quad \rho_{\text{end}} \simeq 0.215 M^2,$$

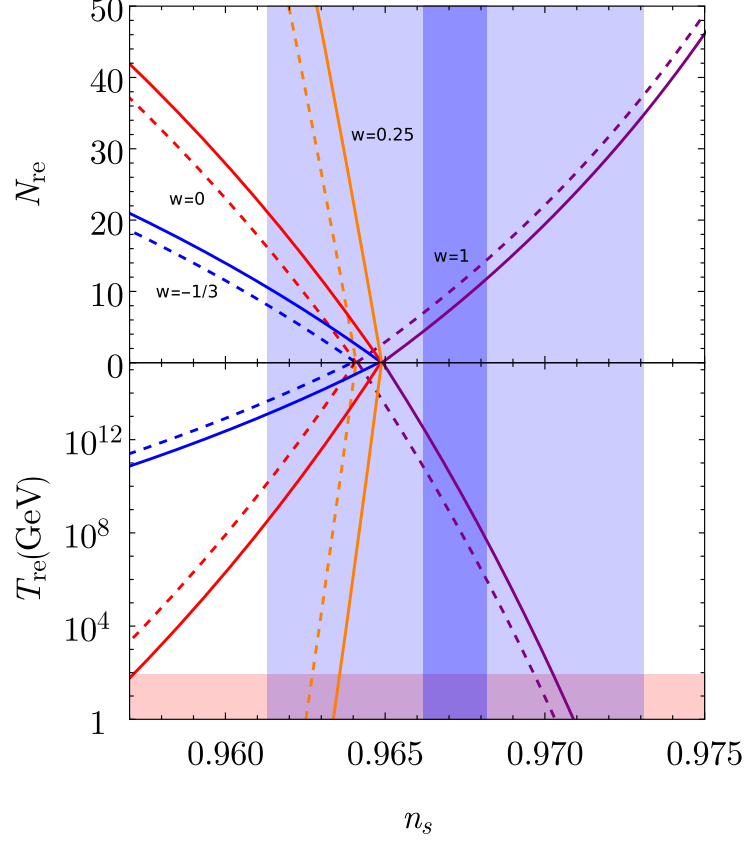


FIG. 4. We plot the duration of reheating  $N_{\text{re}}$  and reheating temperature  $T_{\text{re}}$  given by Eqs. (24) and (25) as function of the scalar spectral index  $n_s$  parametrically for both analytical and numerical solution, given by Eqs. (31) and (16), respectively. The solid lines are for the numerical solution, and the dashed lines are for the analytically approximated solution. Please note that different colors represent dynamics corresponding to different effective equations of state parameter  $w_{\text{re}}$  as indicated in the figure. The blue-shaded region represents the  $1\sigma$  constraint on the value of  $n_s$  using ongoing observations [32–35] with  $n_s = 0.9672 \pm 0.0059$ . The dark blue region shows the future projected bound on  $n_s$  with a sensitivity of  $10^{-3}$ , assuming its central value remains unchanged. The temperature below the lighter red region is excluded due to the constraint from the electroweak scale, which is taken to be 100 GeV.

along with the slow-roll solutions given in Eqs. (30). Here,  $N_{\text{end}}$  is the duration of the field rolling from the initial value  $\phi_i$  to  $\phi_{\text{end}}$ , i.e., the duration of inflation. These values are essential for the analysis in Eqs. (24) and (25) which has been shown in the previous section with Fig. 2.

To improve the analysis, in this section, we now consider, rather than the slow-roll, the full inflationary equations (*viz.* Eqs. (9) and (10)):

$$H = \sqrt{\frac{V}{3 - \frac{1}{2}\phi_N^2}}, \quad \phi_{NN} + \left(3 - \frac{1}{2}\phi_N^2\right) \left(\phi_N + \frac{V_\phi}{\phi}\right) = 0.$$

Solving the highly non-linear differential equation with identical initial condition  $\phi_i = 5.8$ , we now obtain the numerical solutions of the background variables such as the Hubble parameter and the slow-roll parameters along with:

$$N_{\text{end}} \simeq 82.48, \quad \phi_{\text{end}} \simeq 0.61, \quad H_{\text{end}} = 0.241 M, \quad \rho_{\text{end}} \simeq 0.175 M^2.$$

Thus, there is a significant improvement not only in the numerical solution of the background variables but also in  $H_{\text{end}}$ ,  $\rho_{\text{end}}$ , and  $N_{\text{end}}$ . These improvements directly impact the reheating analysis in two ways. The first is the direct influence of  $\rho_{\text{end}}$  in Eq. (24). The second, and more crucial, impact is the significant improvement in  $\Delta N_{\text{end}} = \Delta N_k \sim 1.5$ , which in turn enhances the accuracy of the background variables. For example, in the case of leading order approximations,  $\{\epsilon_1, \epsilon_2\} \simeq \{0.0003, 0.040\}$  for  $N_k = 50$ , whereas, numerically we obtain these values as  $\{\epsilon_1, \epsilon_2\} \simeq \{0.00027, 0.038\}$ , and thus  $\Delta n_s \simeq 2 \times 10^{-3}$ , as also discussed in Ref. [72]<sup>2</sup>.

We now examine the impact of this on the reheating analysis and compare the results with the results obtained using slow-roll approximations. This is illustrated in Fig. 4. As anticipated, the improvement is significant. In the figure, one can see that numerical predictions show a significant shift to the right in the estimates of  $N_{\text{re}}$  and  $T_{\text{re}}$ . Due to this shift, the bound on  $N_k$ , and subsequently  $n_s$  also changes, with an improvement being  $\Delta n_s \sim 10^{-3}$ . For example, in the case of leading-order slow-roll approximation with  $w_{\text{re}} < 1/3$ , the upper bound on  $n_s$  is:  $n_s \leq 0.964$ , whereas, in this improved case, the bound becomes  $n_s \leq 0.965$ . The improvements are explicitly shown in the Table I. This confirms our anticipation that the accurate dynamics help improve the theoretical predictions, which is one of the main results of this work.

## B. Implementation of higher-order slow-roll approximations

In the previous section, we estimated the reheating parameters and e-folding number using the numerical background solution with the leading order inflationary observables, i.e., Eqs. (16).

<sup>2</sup> Please note that, for a multi-parameter model, numerical evaluation for the entire range of the parameters can be challenging. In that case, one can rely upon a semi-analytical solution presented in Ref. [72], where analytically obtained solutions are nearly comparable to the numerical solutions.

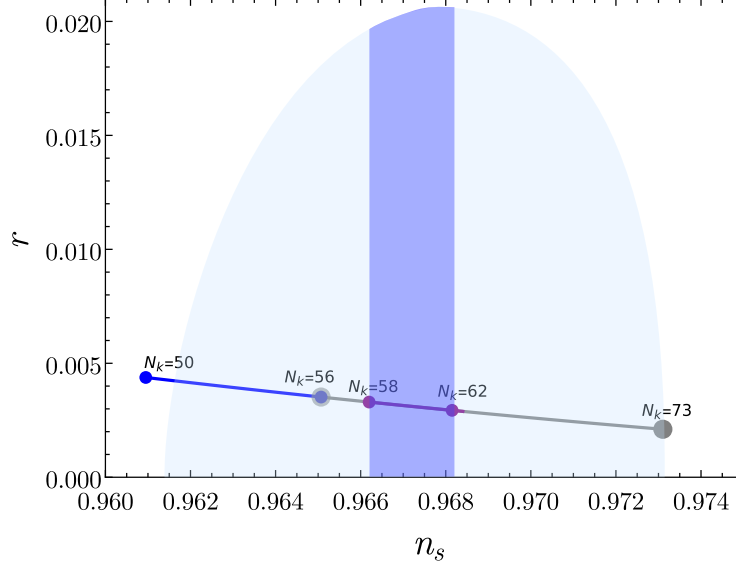


FIG. 5. We plot the inflationary observables, tensor-to-scalar ratio ( $r$ ) as a function of scalar spectral index ( $n_s$ ) for the Starobinsky model using numerical solution given by Eq. (16). This evolution is presented considering the bound on duration  $N_k$  using the reheating regime. We consider different EoS parameters during reheating  $w_{\text{re}}$  and observe the constraint on the duration  $N_k$ . Correspondingly, in the figure, blue line corresponds to the bound for  $w_{\text{re}} < 1/3$ , the gray line for  $w_{\text{re}} > 1/3$  and the purple line for the future observational bound of  $n_s$ . The blue-shaded region represents the  $1\sigma$  constraint on the value of  $n_s$  using ongoing observations [32–35] with  $n_s = 0.9672 \pm 0.0059$ . The dark blue region shows the future projected bound on  $n_s$  with a sensitivity of  $10^{-3}$ , assuming its central value remains unchanged.

However, as mentioned earlier, these expressions are obtained using leading-order slow-roll, and the full solutions of the amplitude of scalar power spectrum, scalar spectral index as well as the tensor-to-scalar ratio in terms of the slow-roll parameter are given as [25, 74]:

$$A_s = 1 - 2(C+1)\epsilon_1 - C\epsilon_2 + \left(2C^2 + 2C + \frac{\pi^2}{2} - f\right)\epsilon_1^2 + \left(C^2 - C + \frac{7\pi^2}{12} - g\right)\epsilon_1\epsilon_2 + \left(\frac{1}{2}C^2 + \frac{\pi^2}{8} - 1\right)\epsilon_2^2 + \left(-\frac{1}{2}C^2 + \frac{\pi^2}{24}\right)\epsilon_2\epsilon_3, \quad (38)$$

$$n_s = 1 - 2\epsilon_1 - \epsilon_2 - 2\epsilon_1^2 - (3 + 2C)\epsilon_1\epsilon_2 - C\epsilon_2\epsilon_3, \quad (39)$$

$$r = 16\epsilon_1(1 + 2C\frac{\epsilon_2}{2}), \quad (40)$$

where  $C = -2 + \ln 2 + \gamma$ , where  $\gamma$  is the Euler constant,  $f = 5$  and  $g = 7$ . In this section, instead of using Eqs. (16), along with the numerical solution, we consider the above expressions for the observable, repeat the reheating analysis, and compare our results with the numerical results obtained in the previous section, which has been illustrated in Figs. 6 and 7 as well as in Table II.

As again can be seen in Fig. 6, there is a further shift in reheating parameters,  $N_{\text{re}}$  and  $T_{\text{re}}$



	Analytical approximations	Numerical solution
$w_{\text{re}} < 1/3$	$52 \leq N_k \leq 56,$ $0.9613 \leq n_s \leq 0.9641$ $N_{\text{re}} \leq 16 \ (w_{\text{re}} = 0),$ $T_{\text{re}} \geq 10^{10} \text{ GeV} \ (w_{\text{re}} = 0)$	$50 \leq N_k \leq 56,$ $0.9613 \leq n_s \leq 0.9649,$ $N_{\text{re}} \leq 21 \ (w_{\text{re}} = 0),$ $T_{\text{re}} \geq 10^8 \text{ GeV} \ (w_{\text{re}} = 0)$
$w_{\text{re}} > 1/3$	$56 \leq N_k \leq 74,$ $0.9641 \leq n_s \leq 0.9731,$ $N_{\text{re}} \leq 37 \ (w_{\text{re}} = 1),$ $T_{\text{re}} \geq 10^{-9} \text{ GeV} \ (w_{\text{re}} = 1)$	$56 \leq N_k \leq 73,$ $0.9649 \leq n_s \leq 0.9731,$ $N_{\text{re}} \leq 34 \ (w_{\text{re}} = 1),$ $T_{\text{re}} \geq 10^{-8} \text{ GeV} \ (w_{\text{re}} = 1)$
future observations $(w_{\text{re}} > 1/3: \text{ allowed})$ $(w_{\text{re}} < 1/3: \text{ not allowed})$	$59 \leq N_k \leq 63,$ $0.9662 \leq n_s \leq 0.9682,$ $7 \leq N_{\text{re}} \leq 14 \ (w_{\text{re}} = 1),$ $10^9 \text{ GeV} \geq T_{\text{re}} \geq 10^6 \text{ GeV} \ (w_{\text{re}} = 1)$	$58 \leq N_k \leq 62,$ $0.9662 \leq n_s \leq 0.9682,$ $4 \leq N_{\text{re}} \leq 12 \ (w_{\text{re}} = 1),$ $10^{12} \text{ GeV} \geq T_{\text{re}} \geq 10^7 \text{ GeV} \ (w_{\text{re}} = 1)$

TABLE I. Starobinsky Inflation: The bounds on variables  $N_k$ ,  $n_s$ ,  $N_{\text{re}}$ , and  $T_{\text{re}}$  for different values of  $w_{\text{re}}$  corresponding to analytically (slow-roll) approximated and the numerical solutions are shown.

compared to the improvements mentioned in the previous section. We obtain an additional improvement of  $\Delta n_s \sim 4 \times 10^{-4}$ , resulting a new bound on  $n_s$  becomes  $n_s \leq 0.9653$  for  $w_{\text{re}} < 1/3$ . Thus, considering higher-order slow-roll approximations instead of the leading-order can significantly improve the estimation of the observables by an order of  $\sim 10^{-3}$ . The detailed bounds on parameters are shown in the Table II.

### C. Implementation of the onset of reheating as the bottom of the potential

Till now, we were estimating  $N_{\text{re}}$  and  $T_{\text{re}}$ , considering the onset of the reheating era after the end of inflation. However, in Ref. [63], it has been shown that, instead of considering minimal gravity theory, if one considers modified gravity theories, the onset of reheating as the end of inflation can make a significant change in the analysis. This is because,  $\epsilon_1$  is not a invariant under conformal transformation. Therefore, in a meaningful manner, one can choose the onset of

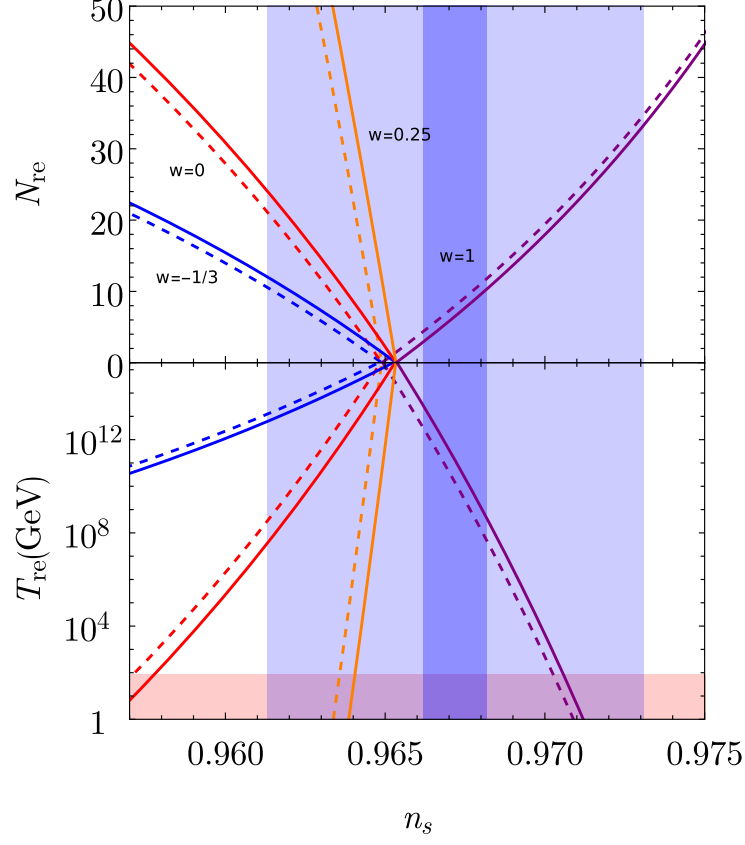


FIG. 6. We plot the duration of reheating  $N_{\text{re}}$  and reheating temperature  $T_{\text{re}}$  given by Eqs. (24) and (25) as function of the scalar spectral index  $n_s$  parametrically comparing numerical solution with leading-order approximations and numerical solution with higher-order approximations given by Eq. (16), (39) respectively. The solid lines are for the higher-order approximations and the dashed lines are for the leading-order approximations. Please note that different colors represent dynamics corresponding to different effective equations of state parameter  $w_{\text{re}}$  as indicated in the figure. The blue-shaded region represents the  $1\sigma$  constraint on the value of  $n_s$  using ongoing observations[32–35] with  $n_s = 0.9672 \pm 0.0059$ . The dark blue region shows the future projected bound on  $n_s$  with a sensitivity of  $10^{-3}$ , assuming its central value remains unchanged. The temperature below the lighter red region is excluded due to the constraint from the electroweak scale, which is taken to be 100 GeV.

reheating as the bottom of the potential, as this point is conformally invariant, and can be used even for general modified gravity theories. Therefore, in this section, we introduce corrections to the reheating analysis, and thus the observables, by considering that the reheating era commences after the epoch at which the potential touches its minima (bottom of the potential). In that case,

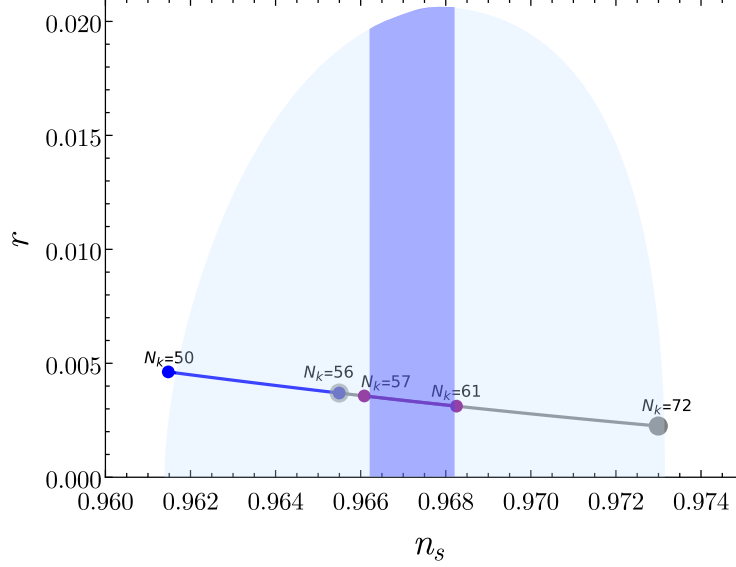


FIG. 7. We plot the inflationary observables, tensor-to-scalar ratio ( $r$ ) as a function of scalar spectral index ( $n_s$ ) for the Starobinsky model using higher-order approximations given by Eq. (39) and (40). This evolution is presented considering the bound on duration  $N_k$  using the reheating regime. We consider different EoS parameters during reheating  $w_{\text{re}}$  and observe the constraint on the duration  $N_k$ . Correspondingly, in the figure, blue line corresponds to the bound for  $w_{\text{re}} < 1/3$ , the gray line for  $w_{\text{re}} > 1/3$  and the purple line for the future observational bound of  $n_s$ . The blue-shaded region represents the  $1\sigma$  constraint on the value of  $n_s$  using ongoing observations [32–35] with  $n_s = 0.9672 \pm 0.0059$ . The dark blue region shows the future projected bound on  $n_s$  with a sensitivity of  $10^{-3}$ , assuming its central value remains unchanged.

Eq. (24) can be re-written as

$$N_{\text{re}} = \frac{4}{1 - 3w_{\text{re}}} \left( -N_k - N_{\text{eb}} - \frac{1}{4} \log \left( \frac{30}{\pi^2 g_{\text{reh}}} \right) - \frac{1}{3} \log \left( \frac{11g_{\text{s, re}}}{43} \right) - \log \left( \frac{k}{a_0 T_0} \right) - \frac{1}{4} \log \rho_b + \log H_k \right), \quad (41)$$

and the reheating temperature, i.e., Eq. (25) can also be evaluated as:

$$T_{\text{re}} = \frac{a_0 T_0}{k} \left( \frac{43}{11g_{\text{s, re}}} \right) e^{-N_k - N_{\text{eb}} - N_{\text{re}}}. \quad (42)$$

Here,  $N_{\text{eb}} \equiv a_b/a_{\text{end}}$  and  $\rho_b \equiv 3H_b^2$ , where ( $b$ ) denotes the bottom of the potential. Again, we perform our analysis considering the numerically obtained solution with higher-order slow-roll corrections and the onset of reheating as the bottom of the potential. However, to our surprise, we find that this implementation does not improve the accuracy to a significant amount, as  $\Delta n_s \sim 10^{-5}$ .

To summarize our cumulative result, in Fig. 8, we plot the results obtained through the analytical approximations mentioned in the first section and the improvement obtained through

	Numerical solution with leading-order $n_s, r$ expressions	Numerical solution with higher-order $n_s, r$ expressions
$w_{\text{re}} < 1/3$	$50 \leq N_k \leq 56,$ $0.9613 \leq n_s \leq 0.9649$ $N_{\text{re}} \leq 21 (w_{\text{re}} = 0),$ $T_{\text{re}} \geq 10^8 \text{ GeV} (w_{\text{re}} = 0)$	$50 \leq N_k \leq 56,$ $0.9613 \leq n_s \leq 0.9653,$ $N_{\text{re}} \leq 24 (w_{\text{re}} = 0),$ $T_{\text{re}} \geq 10^7 \text{ GeV} (w_{\text{re}} = 0)$
$w_{\text{re}} > 1/3$	$56 \leq N_k \leq 73,$ $0.9649 \leq n_s \leq 0.9731,$ $N_{\text{re}} \leq 34 (w_{\text{re}} = 1),$ $T_{\text{re}} \geq 10^{-8} \text{ GeV} (w_{\text{re}} = 1)$	$56 \leq N_k \leq 72,$ $0.9653 \leq n_s \leq 0.9731,$ $N_{\text{re}} \leq 33 (w_{\text{re}} = 1),$ $T_{\text{re}} \geq 10^{-7} \text{ GeV} (w_{\text{re}} = 1)$
future observations ( $w_{\text{re}} > 1/3$ : allowed) ( $w_{\text{re}} < 1/3$ : not allowed)	$58 \leq N_k \leq 62,$ $0.9662 \leq n_s \leq 0.9682,$ $4 \leq N_{\text{re}} \leq 12 (w_{\text{re}} = 1),$ $10^{12} \text{ GeV} \geq T_{\text{re}} \geq 10^7 \text{ GeV} (w_{\text{re}} = 1)$	$57 \leq N_k \leq 61,$ $0.9662 \leq n_s \leq 0.9682,$ $3 \leq N_{\text{re}} \leq 10 (w_{\text{re}} = 1),$ $10^{13} \text{ GeV} \geq T_{\text{re}} \geq 10^8 \text{ GeV} (w_{\text{re}} = 1)$

TABLE II. Starobinsky Inflation: The bounds on variables  $N_k$ ,  $n_s$ ,  $N_{\text{re}}$ , and  $T_{\text{re}}$  for different values of  $w_{\text{re}}$  corresponding to leading-order approximations and the higher-order approximations are shown. Note that, in both cases, the background solutions are numerically obtained.

the implementation of three corrections to the dynamics, and Table III summarizes all the results. Compared to the conventional analytical case, our corrections improve the accuracy in  $n_s$  to  $\Delta n_s \sim 1.2 \times 10^{-3}$ , which is significant. Note that, if the central value of  $n_s$  is assumed to be  $\sim 0.9672$  even in this case, then even with the improvements, the Starobinsky model can indeed be ruled out at  $1\sigma$  level from the expected future observation. These are the main results of this work.

## V. SUMMARY AND CONCLUSIONS

In this article, we consider a single canonical scalar field model minimally coupled to the gravity with a potential  $V(\phi)$  that drives the evolution of the early universe, including both slow-roll

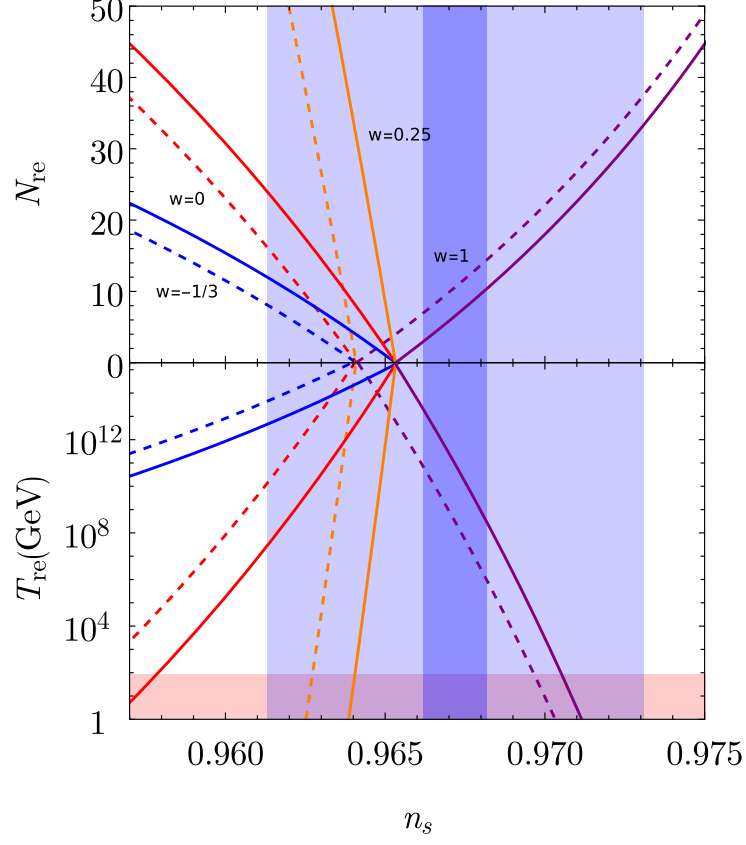


FIG. 8. We plot the duration of reheating  $N_{\text{re}}$  and reheating temperature  $T_{\text{re}}$  given by Eqs. (24) and (25) as function of the scalar spectral index  $n_s$  parametrically comparing analytically approximated solution and numerical solution with higher-order approximations, given by Eqs. (31), (39) respectively. The solid lines are for the onset of reheating as the bottom of the potential and the dashed lines are for the analytically approximated solution. Please note that different colors represent dynamics corresponding to different effective equations of state parameter  $w_{\text{re}}$  as indicated in the figure. The blue-shaded region represents the  $1\sigma$  constraint on the value of  $n_s$  using ongoing observations [32–35] with  $n_s = 0.9672 \pm 0.0059$ . The dark blue region shows the future projected bound on  $n_s$  with a sensitivity of  $10^{-3}$ , assuming its central value remains unchanged. The temperature below the lighter red region is excluded due to the constraint from the electroweak scale, which is taken to be 100 GeV.

inflation and oscillatory solution around the minima of the potential, also known as the reheating epoch. In obtaining the solution, we often use different sets of approximations in both regimes. In the slow-roll inflationary regime, where  $\epsilon_1, \epsilon_2 \ll 1$ , we rely upon the slow-roll approximations. In contrast, the reheating epoch is, for simplicity, quantitatively characterized by the effective EoS parameter  $w_{\text{re}}$  and the duration of this epoch  $N_{\text{re}}$  (or the reheating temperature  $T_{\text{re}}$ ). However, these approximations may lead to a significant discrepancy in the theoretical estimation of the

	Analytical approximations	Higher-order approximations
$w_{\text{re}} < 1/3$	$52 \leq N_k \leq 56,$ $0.9613 \leq n_s \leq 0.9641,$ $N_{\text{re}} \leq 16 \ (w_{\text{re}} = 0),$ $T_{\text{re}} \geq 10^{10} \text{ GeV} \ (w_{\text{re}} = 0)$	$50 \leq N_k \leq 56,$ $0.9613 \leq n_s \leq 0.9653,$ $N_{\text{re}} \leq 24 \ (w_{\text{re}} = 0),$ $T_{\text{re}} \geq 10^7 \text{ GeV} \ (w_{\text{re}} = 0)$
$w_{\text{re}} > 1/3$	$56 \leq N_k \leq 74,$ $0.9641 \leq n_s \leq 0.9731,$ $N_{\text{re}} \leq 37 \ (w_{\text{re}} = 1),$ $T_{\text{re}} \geq 10^{-9} \text{ GeV} \ (w_{\text{re}} = 1)$	$56 \leq N_k \leq 72,$ $0.9653 \leq n_s \leq 0.9731,$ $N_{\text{re}} \leq 33 \ (w_{\text{re}} = 1),$ $T_{\text{re}} \geq 10^{-7} \text{ GeV} \ (w_{\text{re}} = 1)$
future observations ( $w_{\text{re}} > 1/3$ : allowed) ( $w_{\text{re}} < 1/3$ : not allowed)	$59 \leq N_k \leq 63,$ $0.9662 \leq n_s \leq 0.9682,$ $7 \leq N_{\text{re}} \leq 14 \ (w_{\text{re}} = 1),$ $10^9 \text{ GeV} \geq T_{\text{re}} \geq 10^6 \text{ GeV} \ (w_{\text{re}} = 1)$	$57 \leq N_k \leq 61,$ $0.9662 \leq n_s \leq 0.9682,$ $3 \leq N_{\text{re}} \leq 10 \ (w_{\text{re}} = 1),$ $10^{13} \text{ GeV} \geq T_{\text{re}} \geq 10^8 \text{ GeV} \ (w_{\text{re}} = 1)$

TABLE III. Starobinsky Inflation: The bounds on variables,  $N_k$ ,  $n_s$ ,  $N_{\text{re}}$ , and  $T_{\text{re}}$  for different values of  $w_{\text{re}}$  corresponding to analytical approximated parameters, and numerical solution with higher-order approximations are shown.

observables ( $n_s$  and  $r$ ). While accurately defining the reheating epoch (*viz.* the qualitative analysis) is challenging, this work focuses on examining the impact of a more accurate dynamics, rather than the slow-roll approximations, on the perturbed observables.

In order to do this, we specifically considered the following improvements in the dynamics:

1. Numerical Solution: In this method, we solve the complete background Eq. (10) using the numerical method, which provides us with an accurate solution for the dynamics of the universe in its early phase. Using this solution, we estimate the observables and compare the results with the solutions obtained using slow roll approximation.
2. Higher-order approximations: This method includes higher-order slow-roll corrections to the inflationary observables, Eqs. (38), (39) and (40), rather than Eqs. (16). Here also, we used complete numerical solution and estimated the observables using higher order slow-roll corrections and estimated the discrepancy in the observables with respect to the analytical

solution obtained using slow-roll approximation.

3. Onset of the reheating as the bottom of the potential: Typically, the end of inflation is considered the onset of the reheating epoch. However, in this method, we show that if reheating begins at the bottom of the potential, the reheating parameters are modified, as given by Eq. (41) and Eq. (42). This modification can provide a new bound on the duration  $N_k$ , leading to a discrepancy in the scalar spectral index.

After implementing these changes, we found an improvement in the theoretical bounds on the observables. As seen in Fig. 8, there is an improvement of  $\Delta n_s \sim 1.2 \times 10^{-3}$ . These numerical predictions indicate that for  $w_{\text{re}} < 1/3$ , the Starobinsky model has an upper bound as  $n_s \leq 0.9653$ . This can be ruled out from the future observational constraint if the central value is  $n_s \simeq 0.9672$  [35]. However, for  $w_{\text{re}} > 1/3$ , the reheating parameters fall within the future observational bounds, though, at the cost of sufficient reheating e-folding number ( $\sim \mathcal{O}(1-2)$ ). This scenario can again be ruled out if future observations detect instantaneous reheating [92, 93].

The result is compelling, as now it has been established that corrections due to accurate dynamics or higher-order slow-roll approximations can not be ignored. This also implies that even seemingly minor corrections must be considered and implemented to study their implications on perturbed observables. Therefore, when obtaining observational bounds on any inflationary models, one must consider all these corrections, which have been reserved for future endeavors.

In addition to these methods, other improvements can also be made to further enhance the accuracy. For example, in this work, we only considered the slow-roll dynamics, but one could also improve the reheating analysis by incorporating qualitative analysis of the reheating and implementing the changes into the quantitative analysis. Second, higher-order correlation such as non-Gaussianity (see, for instance, Refs. [96–100]) can play a pivotal role in the observables. Third, the implications of primordial black holes and primordial gravitational waves may also play a crucial role in inflationary and post-inflationary dynamics. Fourth, exploring the non-minimal sector instead of the minimal theory of gravity is another avenue. In fact, in our work, while the corrections due to the onset of reheating as the bottom of the potential did not play a significant role, they could be significant in the non-minimal sector [63, 101]. Finally, extending the analysis to non-inflationary dynamics, such as viable classical bounces, is also possible. Recent studies [100, 102–108] show that these alternatives can also fit observations well. Therefore, one must consider all alternatives to slow-roll inflation and carefully study the analysis with all effects, even those that seem minor, to determine the observable constraints of the model.

## ACKNOWLEDGEMENTS

DN is supported by the DST, Government of India through the DST-INSPIRE Faculty fellowship (04/2020/002142). MK is supported by a DST-INSPIRE Fellowship under the reference number: IF170808, DST, Government of India. DN, SY and MK are also very thankful to the Department of Physics and Astrophysics, University of Delhi. MK, SY and DN also acknowledge facilities provided by the IUCAA Centre for Astronomy Research and Development (ICARD), University of Delhi.

- 
- [1] A. A. Starobinsky, JETP Lett. **30**, 682 (1979).
  - [2] A. A. Starobinsky, *Phys. Lett. B* **91**, 99 (1980).
  - [3] A. H. Guth, *Phys. Rev. D* **23**, 347 (1981).
  - [4] K. Sato, *Monthly Notices of the Royal Astronomical Society* **195**, 467 (1981), <http://oup.prod.sis.lan/mnras/article-pdf/195/3/467/4065201/mnras195-0467.pdf>.
  - [5] V. F. Mukhanov and G. V. Chibisov, JETP Lett. **33**, 532 (1981), [Pisma Zh. Eksp. Teor. Fiz.33,549(1981)].
  - [6] A. Linde, *Physics Letters B* **108**, 389 (1982).
  - [7] S. Hawking, *Physics Letters B* **115**, 295 (1982).
  - [8] A. A. Starobinsky, *Phys. Lett. B* **117**, 175 (1982).
  - [9] A. H. Guth and S.-Y. Pi, *Phys. Rev. Lett.* **49**, 1110 (1982).
  - [10] M. Sasaki, *Progress of Theoretical Physics* **76**, 1036 (1986).
  - [11] A. Albrecht and P. J. Steinhardt, *Phys. Rev. Lett.* **48**, 1220 (1982).
  - [12] A. D. Linde, *Phys. Lett.* **129B**, 177 (1983).
  - [13] A. Vilenkin, *Nuclear Physics B* **226**, 527 (1983).
  - [14] J. M. Bardeen, P. J. Steinhardt, and M. S. Turner, *Phys. Rev. D* **28**, 679 (1983).
  - [15] E. W. Kolb and M. Turner, *The early universe* (Reading, Mass. : Addison-Wesley, 1990).
  - [16] V. F. Mukhanov, H. A. Feldman, and R. H. Brandenberger, *Phys. Rept.* **215**, 203 (1992).
  - [17] A. R. Liddle, P. Parsons, and J. D. Barrow, *Phys. Rev. D* **50**, 7222 (1994), [arXiv:astro-ph/9408015](#).
  - [18] J. E. Lidsey, A. R. Liddle, E. W. Kolb, E. J. Copeland, T. Barreiro, *et al.*, *Rev.Mod.Phys.* **69**, 373 (1997), [arXiv:astro-ph/9508078 \[astro-ph\]](#).
  - [19] E. J. Copeland, A. R. Liddle, and D. Wands, *Phys. Rev. D* **57**, 4686 (1998), [arXiv:gr-qc/9711068](#).
  - [20] J. Martin and R. H. Brandenberger, *Phys. Rev. D* **63**, 123501 (2001), [arXiv:hep-th/0005209](#).
  - [21] A. Linde, *arXiv e-prints*, hep-th/0503203 (2005), [arXiv:hep-th/0503203 \[astro-ph\]](#).
  - [22] D. H. Lyth, *22nd IAP Colloquium on Inflation + 25: The First 25 Years of Inflationary Cosmology Paris, France, June 26-30, 2006*, *Lect. Notes Phys.* **738**, 81 (2008), [arXiv:hep-th/0702128 \[hep-th\]](#).



- [23] L. Sriramkumar, (2009), [arXiv:0904.4584 \[astro-ph.CO\]](#).
- [24] D. Baumann, in *Physics of the large and the small, TASI 09, proceedings of the Theoretical Advanced Study Institute in Elementary Particle Physics, Boulder, Colorado, USA, 1-26 June 2009* (2011) pp. 523–686, [arXiv:0907.5424 \[hep-th\]](#).
- [25] J. Martin, C. Ringeval, and V. Vennin, *Phys. Dark Univ.* **5-6**, 75 (2014), [arXiv:1303.3787 \[astro-ph.CO\]](#).
- [26] A. Linde, in *Proceedings, 100th Les Houches Summer School: Post-Planck Cosmology: Les Houches, France, July 8 - August 2, 2013* (2015) pp. 231–316, [arXiv:1402.0526 \[hep-th\]](#).
- [27] J. Martin, *Astrophys. Space Sci. Proc.* **45**, 41 (2016), [arXiv:1502.05733 \[astro-ph.CO\]](#).
- [28] P. Ade *et al.* (Planck), *Astron. Astrophys.* **594**, A20 (2016), [arXiv:1502.02114 \[astro-ph.CO\]](#).
- [29] P. Ade *et al.* (Planck), *Astron. Astrophys.* **594**, A17 (2016), [arXiv:1502.01592 \[astro-ph.CO\]](#).
- [30] S. Clesse, in *10th Modave Summer School in Mathematical Physics* (2015) [arXiv:1501.00460 \[astro-ph.CO\]](#).
- [31] S. D. Odintsov, V. K. Oikonomou, I. Giannakoudi, F. P. Fronimos, and E. C. Lympieriadou, *Symmetry* **15**, 1701 (2023), [arXiv:2307.16308 \[gr-qc\]](#).
- [32] Y. Akrami *et al.* (Planck), *Astron. Astrophys.* **641**, A10 (2020), [arXiv:1807.06211 \[astro-ph.CO\]](#).
- [33] N. Aghanim *et al.* (Planck), *Astron. Astrophys.* **641**, A6 (2020), [Erratum: *Astron. Astrophys.* 652, C4 (2021)], [arXiv:1807.06209 \[astro-ph.CO\]](#).
- [34] P. A. R. Ade *et al.* (BICEP, Keck), *Phys. Rev. Lett.* **127**, 151301 (2021), [arXiv:2110.00483 \[astro-ph.CO\]](#).
- [35] G. Galloni, N. Bartolo, S. Matarrese, M. Migliaccio, A. Ricciardone, and N. Vittorio, *JCAP* **04**, 062, [arXiv:2208.00188 \[astro-ph.CO\]](#).
- [36] A. Albrecht, P. J. Steinhardt, M. S. Turner, and F. Wilczek, *Phys. Rev. Lett.* **48**, 1437 (1982).
- [37] L. F. Abbott, E. Farhi, and M. B. Wise, *Phys. Lett.* **117B**, 29 (1982).
- [38] J. H. Traschen and R. H. Brandenberger, *Phys. Rev. D* **42**, 2491 (1990).
- [39] L. Kofman, A. D. Linde, and A. A. Starobinsky, *Phys. Rev. Lett.* **73**, 3195 (1994), [arXiv:hep-th/9405187 \[hep-th\]](#).
- [40] Y. Shtanov, J. H. Traschen, and R. H. Brandenberger, *Phys. Rev. D* **51**, 5438 (1995), [arXiv:hep-ph/9407247](#).
- [41] L. Kofman, A. D. Linde, and A. A. Starobinsky, *Phys. Rev. D* **56**, 3258 (1997), [arXiv:hep-ph/9704452 \[hep-ph\]](#).
- [42] B. A. Bassett, S. Tsujikawa, and D. Wands, *Rev. Mod. Phys.* **78**, 537 (2006), [arXiv:astro-ph/0507632 \[astro-ph\]](#).
- [43] R. Allahverdi, R. Brandenberger, F.-Y. Cyr-Racine, and A. Mazumdar, *Ann. Rev. Nucl. Part. Sci.* **60**, 27 (2010), [arXiv:1001.2600 \[hep-th\]](#).
- [44] J. Martin and C. Ringeval, *Phys. Rev. D* **82**, 023511 (2010), [arXiv:1004.5525 \[astro-ph.CO\]](#).
- [45] J. Mielczarek, *Phys. Rev. D* **83**, 023502 (2011), [arXiv:1009.2359 \[astro-ph.CO\]](#).

- [46] M. A. Amin, M. P. Hertzberg, D. I. Kaiser, and J. Karouby, *Int. J. Mod. Phys. D* **24**, 1530003 (2014), [arXiv:1410.3808 \[hep-ph\]](#).
- [47] L. Dai, M. Kamionkowski, and J. Wang, *Phys. Rev. Lett.* **113**, 041302 (2014), [arXiv:1404.6704 \[astro-ph.CO\]](#).
- [48] J. Martin, C. Ringeval, and V. Vennin, *Phys. Rev. Lett.* **114**, 081303 (2015), [arXiv:1410.7958 \[astro-ph.CO\]](#).
- [49] V. Domcke and J. Heisig, *Phys. Rev. D* **92**, 103515 (2015), [arXiv:1504.00345 \[astro-ph.CO\]](#).
- [50] J. L. Cook, E. Dimastrogiovanni, D. A. Easson, and L. M. Krauss, *JCAP* **1504**, 047, [arXiv:1502.04673 \[astro-ph.CO\]](#).
- [51] D. Maity and P. Saha, (2016), [arXiv:1610.00173 \[astro-ph.CO\]](#).
- [52] K. D. Lozanov and M. A. Amin, *Phys. Rev. Lett.* **119**, 061301 (2017), [arXiv:1608.01213 \[astro-ph.CO\]](#).
- [53] R. Kabir, A. Mukherjee, and D. Lohiya, *Mod. Phys. Lett. A* **34**, 1950114 (2019), [arXiv:1609.09243 \[gr-qc\]](#).
- [54] D. Maity and P. Saha, (2018), [arXiv:1811.11173 \[astro-ph.CO\]](#).
- [55] D. Maity and P. Saha, *Class. Quant. Grav.* **36**, 045010 (2019), [arXiv:1902.01895 \[gr-qc\]](#).
- [56] K. El Bourakadi, (2021), [arXiv:2104.10552 \[gr-qc\]](#).
- [57] S. D. Odintsov and T. Paul, *Phys. Dark Univ.* **42**, 101263 (2023), [arXiv:2305.19110 \[gr-qc\]](#).
- [58] G. German, J. C. Hidalgo, and L. E. Padilla, *Eur. Phys. J. Plus* **139**, 302 (2024), [arXiv:2310.05221 \[astro-ph.CO\]](#).
- [59] J. B. Munoz and M. Kamionkowski, *Phys. Rev. D* **91**, 043521 (2015), [arXiv:1412.0656 \[astro-ph.CO\]](#).
- [60] J. Martin and C. Ringeval, *JCAP* **0608**, 009, [arXiv:astro-ph/0605367 \[astro-ph\]](#).
- [61] P. Adshead, R. Easther, J. Pritchard, and A. Loeb, *JCAP* **02**, 021, [arXiv:1007.3748 \[astro-ph.CO\]](#).
- [62] J.-O. Gong, S. Pi, and G. Leung, *JCAP* **1505** (05), 027, [arXiv:1501.03604 \[hep-ph\]](#).
- [63] D. Nandi and P. Saha, (2019), [arXiv:1907.10295 \[gr-qc\]](#).
- [64] A. R. Liddle and S. M. Leach, *Phys. Rev. D* **68**, 103503 (2003), [arXiv:astro-ph/0305263 \[astro-ph\]](#).
- [65] P. Andre *et al.* (PRISM), (2013), [arXiv:1306.2259 \[astro-ph.CO\]](#).
- [66] L. Amendola *et al.* (Euclid Theory Working Group), *Living Rev. Rel.* **16**, 6 (2013), [arXiv:1206.1225 \[astro-ph.CO\]](#).
- [67] Y. Mao, M. Tegmark, M. McQuinn, M. Zaldarriaga, and O. Zahn, *Phys. Rev. D* **78**, 023529 (2008), [arXiv:0802.1710 \[astro-ph\]](#).
- [68] F. Finelli *et al.* (CORE), *JCAP* **1804**, 016, [arXiv:1612.08270 \[astro-ph.CO\]](#).
- [69] J. Martin, C. Ringeval, and R. Trotta, *Phys. Rev. D* **83**, 063524 (2011), [arXiv:1009.4157 \[astro-ph.CO\]](#).
- [70] J. Martin, C. Ringeval, R. Trotta, and V. Vennin, *JCAP* **1403**, 039, [arXiv:1312.3529 \[astro-ph.CO\]](#).
- [71] J. Martin, C. Ringeval, and V. Vennin, *JCAP* **1410** (10), 038, [arXiv:1407.4034 \[astro-ph.CO\]](#).
- [72] M. Kaur, D. Nandi, and S. R. B., *JCAP* **05**, 045, [arXiv:2309.10570 \[astro-ph.CO\]](#).
- [73] P. Auclair, B. Blachier, and C. Ringeval, (2024), [arXiv:2406.14152 \[astro-ph.CO\]](#).
- [74] Q.-G. Huang, *Phys. Rev. D* **76**, 043505 (2007), [arXiv:astro-ph/0610924](#).

- [75] C. Caprini, S. H. Hansen, and M. Kunz, *Mon. Not. Roy. Astron. Soc.* **339**, 212 (2003), [arXiv:hep-ph/0210095](#).
- [76] J. M. Cline and L. Hoi, *JCAP* **06**, 007, [arXiv:astro-ph/0603403](#).
- [77] Q.-G. Huang and M. Li, *Nucl. Phys. B* **755**, 286 (2006), [arXiv:astro-ph/0603782](#).
- [78] Q.-G. Huang, *JCAP* **11**, 004, [arXiv:astro-ph/0610389](#).
- [79] H. Peiris and R. Easther, *JCAP* **07**, 002, [arXiv:astro-ph/0603587](#).
- [80] R. Easther and H. Peiris, *JCAP* **09**, 010, [arXiv:astro-ph/0604214](#).
- [81] H. Peiris and R. Easther, *JCAP* **10**, 017, [arXiv:astro-ph/0609003](#).
- [82] K. I. Izawa, *Phys. Lett. B* **576**, 1 (2003), [arXiv:hep-ph/0305286](#).
- [83] A. Ashoorioon, J. L. Hovdebo, and R. B. Mann, *Nucl. Phys. B* **727**, 63 (2005), [arXiv:gr-qc/0504135](#).
- [84] G. Ballesteros, J. A. Casas, and J. R. Espinosa, *JCAP* **03**, 001, [arXiv:hep-ph/0601134](#).
- [85] M. Li, *JCAP* **10**, 003, [arXiv:astro-ph/0607525](#).
- [86] B. Chen, M. Li, T. Wang, and Y. Wang, *Mod. Phys. Lett. A* **22**, 1987 (2007), [arXiv:astro-ph/0610514](#).
- [87] V. Vennin, K. Koyama, and D. Wands, *JCAP* **11**, 008, [arXiv:1507.07575 \[astro-ph.CO\]](#).
- [88] A. Karam, T. Pappas, and K. Tamvakis, *Phys. Rev. D* **96**, 064036 (2017), [arXiv:1707.00984 \[gr-qc\]](#).
- [89] A. A. Starobinsky, *Sov. Astron. Lett.* **9**, 302 (1983).
- [90] A. A. Starobinsky and H. J. Schmidt, *Class. Quant. Grav.* **4**, 695 (1987).
- [91] S. Koh, B.-H. Lee, and G. Tumurtushaa, *Phys. Rev. D* **98**, 103511 (2018), [arXiv:1807.04424 \[astro-ph.CO\]](#).
- [92] J. de Haro, *Phys. Rev. D* **107**, 123511 (2023), [arXiv:2304.05903 \[gr-qc\]](#).
- [93] G. N. Felder, L. Kofman, and A. D. Linde, *Phys. Rev. D* **59**, 123523 (1999), [arXiv:hep-ph/9812289](#).
- [94] P. Andre *et al.* (PRISM), (2013), [arXiv:1306.2259 \[astro-ph.CO\]](#).
- [95] L. Amendola *et al.* (Euclid Theory Working Group), *Living Rev. Rel.* **16**, 6 (2013), [arXiv:1206.1225 \[astro-ph.CO\]](#).
- [96] J. M. Maldacena, *JHEP* **0305**, 013, [arXiv:astro-ph/0210603 \[astro-ph\]](#).
- [97] D. Nandi and S. Shankaranarayanan, *JCAP* **06**, 038, [arXiv:1512.02539 \[gr-qc\]](#).
- [98] D. Nandi and S. Shankaranarayanan, *JCAP* **10**, 008, [arXiv:1606.05747 \[gr-qc\]](#).
- [99] D. Nandi, (2017), [arXiv:1707.02976 \[gr-qc\]](#).
- [100] D. Nandi and L. Sriramkumar, *Phys. Rev. D* **101**, 043506 (2020), [arXiv:1904.13254 \[gr-qc\]](#).
- [101] D. Nandi, *Phys. Rev. D* **99**, 103532 (2019), [arXiv:1904.00153 \[gr-qc\]](#).
- [102] D. Nandi, *JCAP* **05**, 040, [arXiv:1811.09625 \[gr-qc\]](#).
- [103] R. Kothari and D. Nandi, *JCAP* **10**, 026, [arXiv:1901.06538 \[astro-ph.CO\]](#).
- [104] D. Nandi, *Phys. Lett. B* **809**, 135695 (2020), [arXiv:2003.02066 \[astro-ph.CO\]](#).
- [105] D. Nandi, *Universe* **7**, 62 (2021), [arXiv:2009.03134 \[gr-qc\]](#).
- [106] D. Nandi and M. Kaur, (2022), [arXiv:2206.08335 \[astro-ph.CO\]](#).
- [107] D. Nandi and M. Kaur, *Phys. Dark Univ.* **44**, 101430 (2024), [arXiv:2302.03413 \[astro-ph.CO\]](#).

- [108] M. Kaur, D. Nandi, D. Choudhury, and T. R. Seshadri, *Int. J. Mod. Phys. D* **33**, 2450006 (2024), [arXiv:2302.13698 \[astro-ph.CO\]](#).